(Received 3 March 2026, Accepted 10 April 2026, Scheduled 24 April 2026)

A 3D Vertically-Integrated Wideband Filter Antenna for X-Band Applications

Tao Fang, Tao Tang*, Xiangyan Zhao, and Wei Hu

College of Electronics and Information, Southwest Minzu University, Chengdu 610225, China

ABSTRACT: This paper presents a compact wideband integrated filter antenna for X-band applications enabled by a three-dimensional (3D) vertical-interconnect architecture. A self-packaged electromagnetic platform is constructed on a multilayer substrate with a central air cavity, realizing high-density monolithic integration of a slotted patch radiator and a seventh-order microstrip bandpass filter (BPF). Distinct from conventional planar cascaded filtering antennas, the proposed 3D collaborative electromagnetic structure — formed by the air cavity, a perimeter vertical-interconnect access (VIA) array, and multilayer ground planes — provides low-loss signal transmission and effectively suppresses parasitic coupling within a compact volume. To enhance radiation performance, the patch is co-optimized through VIA slot loading, chamfering, and asymmetric feeding to extend the surface-current path, lower the resonant frequency, and broaden the impedance bandwidth, achieving a 45.27% reduction in patch area relative to the initial design. To accommodate the BPF within the packaging boundary, spatial adaptation and impedance matching are achieved through a tilted layout, arc-shaped port extension, and vertical feed VIAs while maintaining essentially unchanged electrical performance. Measured results demonstrate a 40.3% fractional bandwidth from 7.99 to 12.02 GHz, a peak gain of 6.85 dBi, good out-of-band/harmonic suppression, and stable radiation patterns. The overall size is $1.17\lambda_0 \times 1.17\lambda_0 \times 0.12\lambda_0$. The proposed 3D vertical-interconnect and multifunctional self-packaged co-design methodology offers an effective solution for broadband, miniaturized, high-isolation filtering antennas and system-on-package (SoP) RF front ends.

1. INTRODUCTION

The relentless advancement of wireless communication technology has spurred a growing trend towards developing dual-function or multi-function modules to achieve circuit miniaturization and enhanced overall performance [1]. Among the core components of a radio frequency (RF) front-end, filters and antennas are particularly critical, as their performance directly dictates the efficacy of the entire communication system [2–4]. The integration of these two components into a single device, referred to as a filter antenna, has emerged as a promising solution. This approach not only effectively reduces the system footprint but also offers the potential for higher performance and lower insertion loss than discrete counterparts. Consequently, filter antennas have attracted significant research attention in response to the escalating demands for circuit integration and miniaturization [5].

Various design methodologies for filter antennas have been explored in the literature. One prominent category is the direct cascade scheme [6–11], which connects a separate filter to an antenna. While this method offers flexibility in meeting diverse specifications, it often suffers from inherent challenges. A primary issue is impedance mismatch between the filter and antenna, which can lead to performance degradation. Although techniques such as introducing stub lines can fine-tune the matching, this approach typically necessitates intricate matching networks and introduces notable transmission line losses, ultimately compromising the system efficiency.

A second methodology involves transforming the last resonator of a filter into a radiating element, thereby intrinsically merging the filtering and radiation functions [12–17]. This strategy enhances integration and inherently circumvents impedance mismatch issues. However, a key trade-off exists: since the filter's selectivity is governed by its order, high-performance designs often require multiple resonators, resulting in larger overall dimensions. Furthermore, the insertion loss of the filter section directly reduces the antenna's radiation efficiency and gain.

A third common approach entails introducing structural modifications to the antenna itself to generate filtering responses. Techniques such as etching slots [18–20], employing short-circuit pins [21, 22], utilizing stacked patches [23], and adding parasitic strips [24, 25] fall into this category. For instance, gains up to 9.7 dBi have been achieved using a combination of stacked patches, a U-shaped slot, and shorting pins [26]. Defective ground structures (DGSs) [20] and metasurface loads [21, 27] have also been successfully employed to realize high-gain filter antennas. Despite their performance, many of these designs, including some intended for base station applications [19, 25], often exhibit structural complexity, which can hinder fabrication and increase cost.

While various strategies exist to realize filter antennas, many confront inherent trade-offs among performance, size, and complexity. This work adopts a distinct approach by monolithically integrating a seventh-order microstrip bandpass filter (BPF) with a slotted patch antenna in a three-dimensional (3D) vertical-interconnection structure. In this way, the radiator reported in [28] is transformed into a complete filter antenna

* Corresponding author: Tao Tang (tangt@swun.edu.cn).

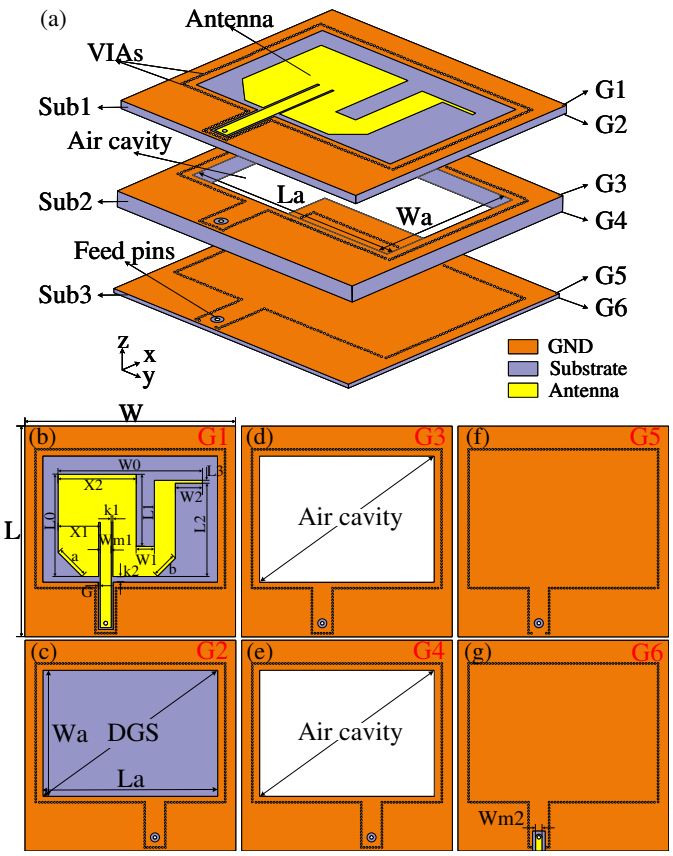

FIGURE 1. Configurations of the antenna(unit: mm). (a) 3D side view of the design. (b) Coplanar waveguide (CPW) G1 with antenna radiation patch. (c) Defect ground structure (DGS) G2 of the antenna. (d) Top ground G3 of the air cavity. (e) Bottom ground G4 of the air cavity. (f) Ground of the filter G5. (g) Ground G6 with the filter.

system. This co-design leverages a multilayer architecture that allows for the independent optimization of components [29], transforming a conventional 2D layout into a compact 3D stack to maximize space utilization and reduce the device footprint. By exploiting the low-loss characteristics of this 3D packaged structure, together with the air cavity and VIA shielding wall for enhanced isolation, the design maintains good radiation performance and competitive gain even with low-cost FR4 substrates used in part of the structure [30], while also minimizing transmission line losses. The resultant prototype exhibits exceptional performance, including a 40.3% operating bandwidth (7.99–12.02 GHz), a peak gain of 6.85 dBi, and crucially, strong harmonic suppression within a compact footprint of $1.17\lambda_0 \times 1.17\lambda_0 \times 0.12\lambda_0$ (λ_0 corresponds to 10 GHz). This work validates the 3D vertical-integration platform as a potent solution for developing high-performance filter antennas that offer a superior balance among wide bandwidth, effective filtering, and compact size for modern X-band wireless systems.

2. CONFIGURATION AND RESULTS

2.1. Antenna Design

The antenna configuration in this design is shown in Fig. 1 and comprises three layers of dielectric substrates, labeled as sub1, sub2, and sub3. Substrates sub1 and sub2 are composed of FR4 material, characterized by a dielectric constant of 4.4 and a loss tangent of 0.02, with thicknesses $H_1 = 1$ mm and $H_2 = 2$ mm, respectively. Substrate sub3 is made of Rogers 4350, featuring a dielectric constant of 3.66, a loss tangent of 0.004, and a thickness $H_3 = 0.508$ mm. To create the air cavity, a rectangular area is excavated from sub2, with dimensions L_a in length and W_a in width. The upper and lower surfaces of each substrate are copper-clad, resulting in six metal layers, designated as G1 to G6 from top to bottom. All layers are connected by VIAs, forming an equivalent electric shorting wall around the air cavity to minimize dielectric loss and effectively shield against external electromagnetic interference.

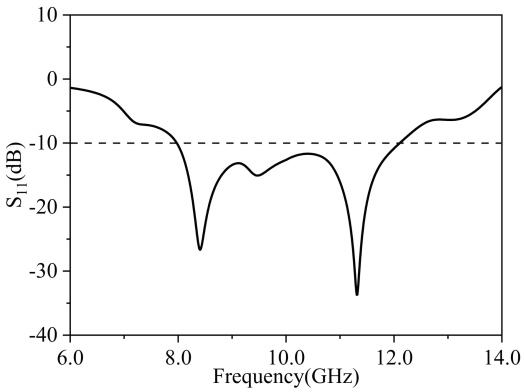

FIGURE 2. Simulated S_{11} in dB of the antenna.

The top layer of sub1 features a patch radiator with slots, chamfer cuts, and an asymmetric feeding line. To integrate with the air cavity positioned directly beneath the radiation patch, the ground plane with DGS on the backside of sub1 is moved to be coplanar with the radiation patch, forming a monopole antenna with CPW feed. G1, G2, the air cavity covered by G3 and G4, all VIAs, and sub3 with G5 and G6 form an integrated package structure of the antenna. The specific dimensions are illustrated in Fig. 1(b), with parameters as $W = L = 35$ mm, $W_a = 20.92$ mm, $W_0 = 24$ mm, $W_1 = 3$ mm, $W_2 = 4.5$ mm, $W_{m1} = 1.85$ mm, $L_a = 29$ mm, $L_0 = 17$ mm, $L_1 = 12$ mm, $L_2 = 15.5$ mm, $L_3 = 0.5$ mm, $K_1 = 0.25$ mm, $K_2 = G = 0.29$ mm, $X_1 = 7$ mm, $X_2 = 13$ mm, $a = 5.66$ mm, and $b = 4.24$ mm. In addition, the radius of each VIA is 0.15 mm (i.e., the diameter is 0.30 mm), and the center-to-center spacing between adjacent VIAs is 0.5 mm.

New resonances are introduced by the CPW and air cavity, together with the monopole and DGS, thereby producing a wideband response. The grounds G5 and G6 at the bottom of the air cavity function as a reflector, reflecting the backward radiation of the antenna to form a directional radiation effect. The simulation result of return loss S_{11} (dB) is shown in Fig. 2. The simulated results show that the proposed antenna operates over 7.97–12.11 GHz, covering the X-band and achieving a fractional bandwidth of 41.24%. Figs. 3(a) to (d) show the radiation patterns of the antenna at different frequencies. It can be seen that the antenna radiation direction has a certain directivity along the z-axis and a maximum gain of 6.41 dBi at 11.5 GHz.

The next subsection presents the integration of a bandpass filter with this antenna core to realize the proposed filter antenna system.

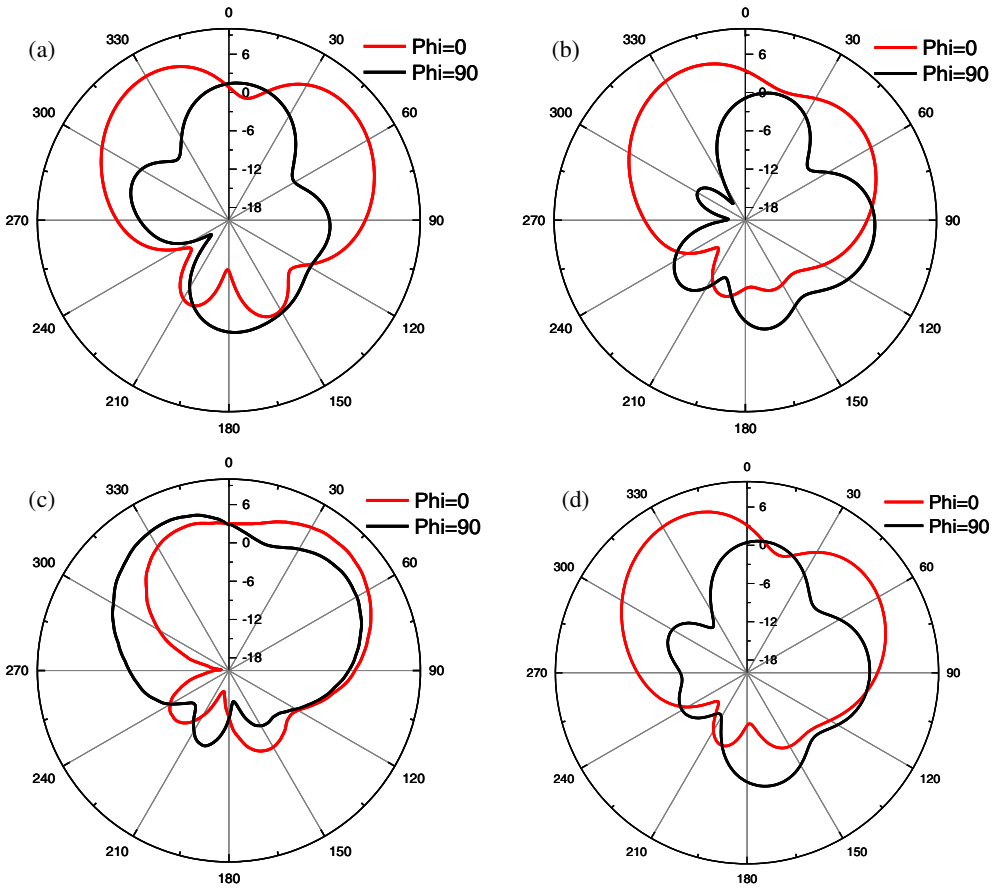

FIGURE 3. Radiation patterns. (a) At 8.5 GHz. (b) At 9 GHz. (c) At 10 GHz. (d) At 11.5 GHz.

2.2. Filter Design

The bandpass filter (BPF) is realized through a parallel-coupled microstrip line structure. The order of the BPF is determined from the prototype of a low-pass filter. The parallel-coupled microstrip line can be regarded as a superposition of even-mode excitation and odd-mode excitation. The even-mode and odd-mode excitations have different characteristic impedances, which are related to the size and material of the microstrip line. When the length of the parallel-coupled microstrip line is $L = \lambda_g/4$, it has the characteristics of bandpass filtering, and multiple coupled microstrip line elements can be cascaded to obtain good filtering characteristics.

Here, a seventh-order coupled resonator is employed to achieve out-of-band suppression for the BPF. The BPF is designed on the Rogers 4350 with a thickness of 0.508 mm, and its size is $37.36 \times 8 \times 0.508\,\text{mm}^3$. The specific structure of the filter is depicted in Fig. 4(a), with parameters as $W_s = 37.36$ mm, $L_s = 8$ mm, $W_{50} = 21.08$ mm, $L_{50} = 3$ mm, $W_{s1} = 0.2$ mm, $W_{s2} = 0.35$ mm, $W_{s3} = 0.45$ mm, $W_{s4} = 0.3$ mm, $L_{s1} = L_{s2} = L_{s3} = L_{s4} = 4.48$ mm, $S_1 = S_2 = S_3 = 0.1$ mm, and $S_4 = 0.2$ mm. The S-parameter simulation results are illustrated in Fig. 4(b). The simulation results indicate that the center frequency of the filter is 10.04 GHz, with a relative -3 dB passband of 42.37% (from 7.91 to 12.17 GHz). The in-band insertion loss is less than 0.5 dB, and the 30 dB/3 dB rectangle coefficient is 1.42. The insertion loss is -35 dB at 7 GHz and -25 dB at 13 GHz, respectively.

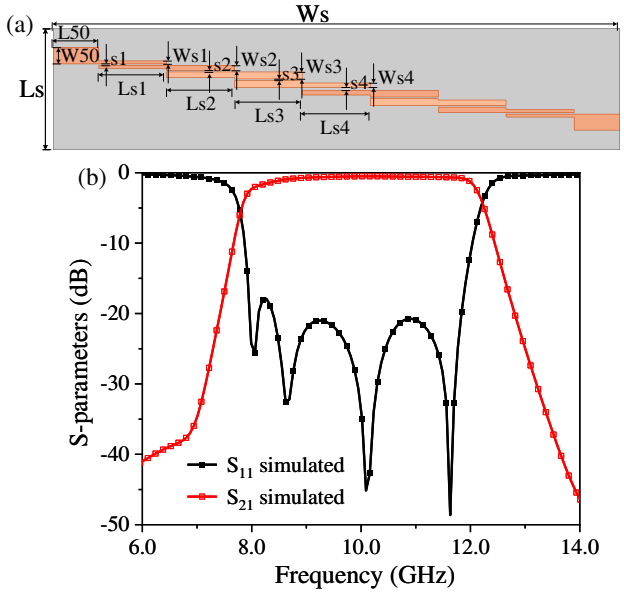

FIGURE 4. Configuration of the filter and results. (a) Configuration. (b) S-parameters.

2.3. Filtering Antenna Design

The integrated design combines the aforementioned antenna with a seventh-order parallel-coupled microstrip bandpass filter (BPF), resulting in a full-fledged filter antenna. The BPF is directly fabricated on the bottom-most metal layer (G6). A

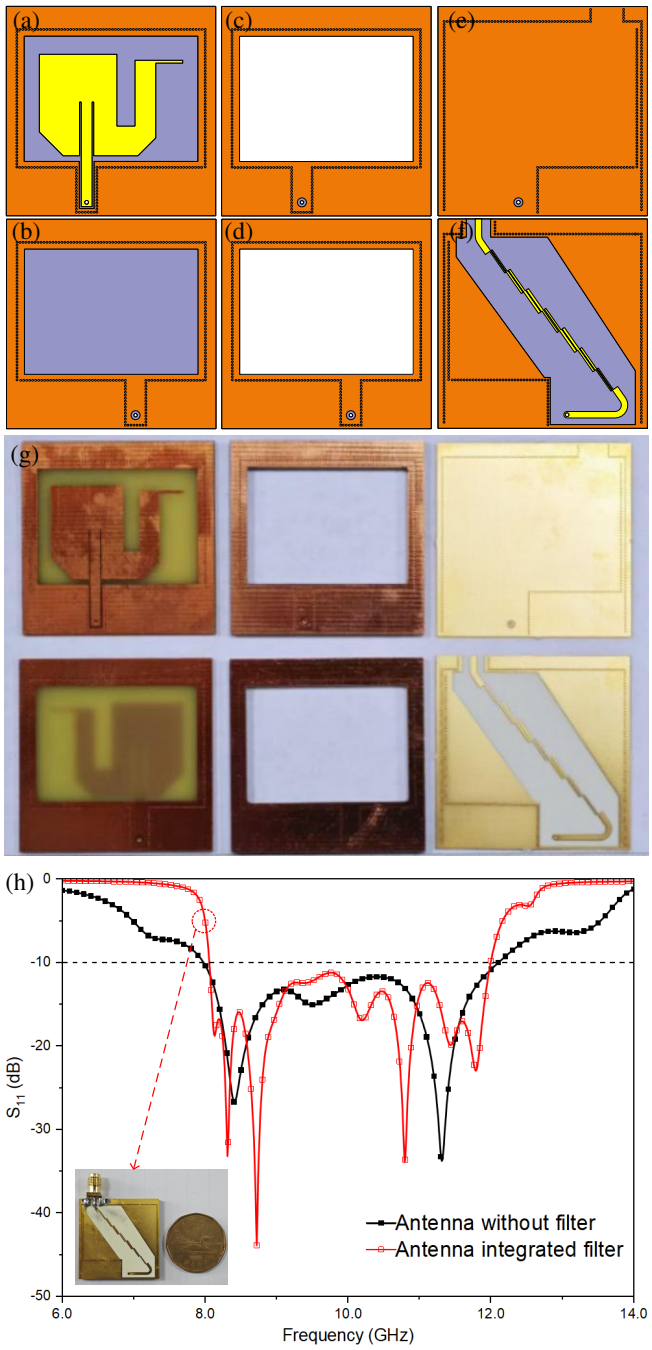

FIGURE 5. Configurations, photos, and results of the Filtering Antenna. (a) to (f) correspond to those depicted in Figs. 1 (b) to (g). (g) Displays photos of each layer. (h) Compare with the S_{11} of the antenna without the BPF and after integration with the BPF.

key design challenge was accommodating the filter's physical length ($W_s = 37.36$ mm) within the antenna's footprint ($W = 35$ mm). To resolve this without compromising electrical performance, two strategic adaptations were employed: first, the filter is placed at a precise angle on the substrate; second, the input and output ports are extended using arc chamfering. This approach effectively reduces the projected horizontal length while maintaining the electrical length of the coupled-line resonators.

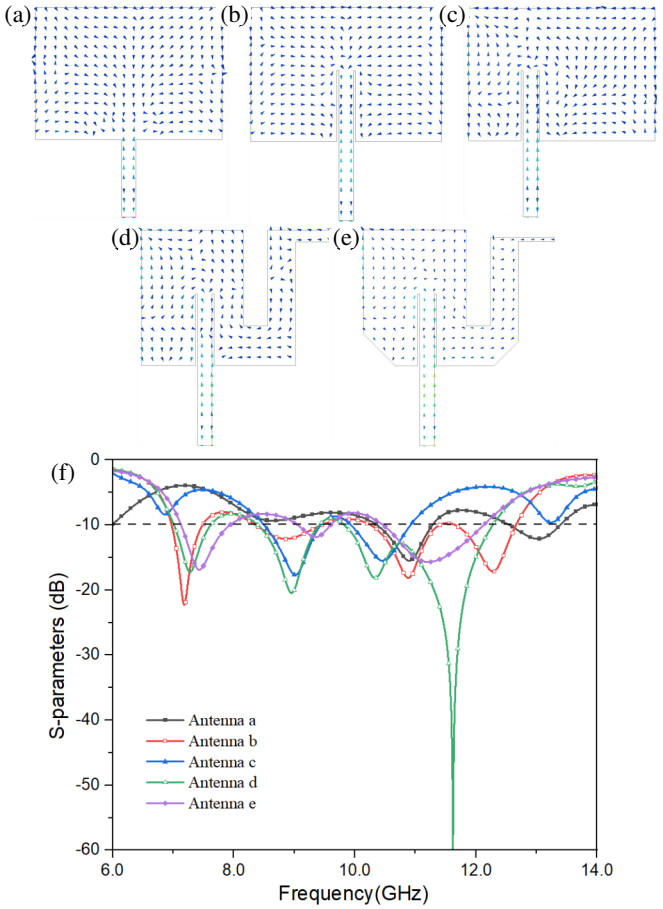

FIGURE 6. Evolution of the antenna with surface current distribution. (a) Initial rectangular antenna. (b) With a feeder gap for matching. (c) Asymmetric feeding. (d) Slots loading on the patch. (e) Chamfer cuts on the patch. (f) Simulated S_{11} responses of Antennas a–e.

The interconnection between the filter's output and the antenna's feed port is achieved through a vertical feed VIA. To prevent an electrical short as this VIA passes through the intermediate ground planes (G5, G4, G3, G2), circular isolation rings with an optimized radius of 0.3 mm are incorporated into these layers. This intricate vertical-interconnect strategy facilitates compact integration and enables precise impedance matching between the two components by adjusting the ring radii and VIA position [31]. Furthermore, the perimeter VIAs, in conjunction with the air cavity and the multi-layer grounds, form an enhanced electromagnetic shielding wall. This 3D packaged structure significantly improves front-to-back isolation, advantages that were not fully leveraged in the context of a passive antenna design like the one in [28].

The configuration and photos of each layer and the side view of the design are depicted in Figs. 5(a)–(g). The system-level benefit of this integration is demonstrated in Fig. 5(h). While the standalone antenna exhibits a broad impedance bandwidth, the integrated filter antenna's operational band is precisely defined by the BPF's passband (8.06–11.99 GHz in simulation). This results in the critical addition of a strong out-of-band rejection capability, a defining feature of the present integrated system that enables the suppression of noise and interference in practical wireless applications.

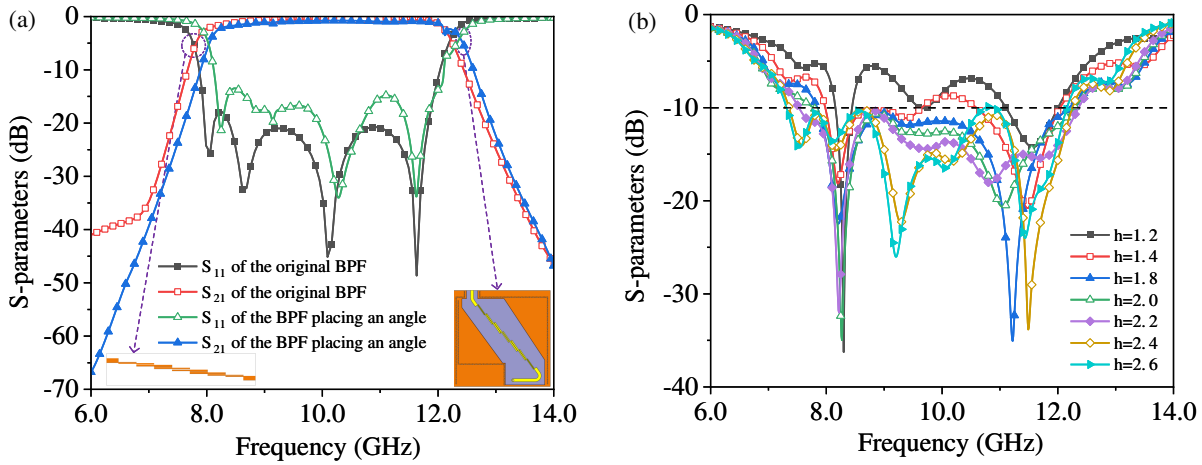

FIGURE 7. S-parameter responses of the antenna and the BPF under varied configurations. (a) Influence of angular placement on the BPF. (b) Effect of air-cavity height on the antenna.

3. DISCUSSIONS

The radiator is initially designed as a CPW-fed monopole-like patch radiator. By strategically modifying the feeding position and introducing slots on the patch, the equivalent current path is extended.As a result, the antenna resonates at a lower frequency than a conventional rectangular patch of similar size, which helps reduce the antenna area. Fig. 6 illustrates the evolutionary progression of the antenna designs along with the corresponding surface current distributions on the radiation patch. In this design evolution, Antenna a serves as the reference prototype, whereas Antennas b–e incorporate slots, chamfer cuts, and asymmetric features to optimize the current path on the radiating patch. These enhancements effectively lower the resonant frequency, contributing to antenna miniaturization.

Figure 6(f) illustrates the S_{11} responses for the various evolutionary stages of the antenna designs. The results reveal that Antenna b introduces a feeder gap for impedance matching, which improves the input matching and broadens the operating bandwidth. Antenna c adopts an asymmetric feed by shifting the feed line to one side of the radiating patch, thereby extending the current path and lowering the resonant frequency, which contributes to antenna miniaturization. Antenna d further improves the design by introducing additional slots into the radiating patch, which increases the effective current path while maintaining the resonant frequency and reducing the antenna size. Antenna e introduces chamfer cuts and narrows the upper branch of the patch, achieving further size reduction without compromising the operating bandwidth.

This analysis demonstrates that Antennas b through e exhibit superior bandwidth and resonant frequency characteristics compared to the original Antenna a. Notably, Antennas d and e achieve comparable operational bandwidths, with Antenna e offering additional size reduction. This evolutionary progression underscores the efficacy of structural modifications in enhancing antenna performance and facilitating miniaturization.

Figure 7(a) presents the S-parameter responses (S_{11} and S_{21}) of the BPF under various configurations, comparing the original design with the BPF positioned at an angle on the substrate and featuring arc chamfering at the port, as shown in Fig. 5(f). The results indicate that tilting the BPF and slightly curving the port lead to a narrower passband and a slight shift toward higher frequencies, while the overall performance remains largely unaffected. This observation suggests that such modifications can be used to satisfy footprint constraints without significantly degrading the BPF performance.

Figure 7(b) presents simulated results showing the influence of the air-cavity height (i.e., the thickness of sub2) on the antenna bandwidth, as reflected by the S_{11} response. The results reveal that the S_{11} performance initially improves with increasing air-cavity height but degrades beyond a certain point. The optimal S_{11} performance is observed at a cavity height of $H = 2$ mm, indicating this configuration as the most effective for achieving the desired antenna performance.

4. MEASUREMENT

The prototypes of the antenna, BPF, and integrated filter antenna were fabricated and subsequently measured. Fig. 8 presents the measurement setup for the S-parameters of the antenna and the BPF, as well as the radiation patterns of the filter antenna.

The performances of the antenna, the filter, and the integrated filter antenna were evaluated by comparing the simulated and measured results, as shown in Fig. 9. The results depicted in Fig. 9(a) indicate a high degree of correlation between the simulated and measured S_{11} parameters of the antenna, thereby validating the accuracy of the antenna design. Fig. 9(b) presents the simulated and measured S_{11} and S_{21} parameters for the filter response. The measured results confirm the filter's excellent performance, with a passband insertion loss of less than 1.5 dB and an out-of-band rejection level better than 15 dB over the measured frequency range.

The measured results reveal a slight broadening of the passband in the higher frequency range, indicating an improvement in the filter's high-frequency performance. Fig. 9(c) displays the simulated and measured S_{11} parameters for the integrated filter antenna system. It is observed that the operational band-

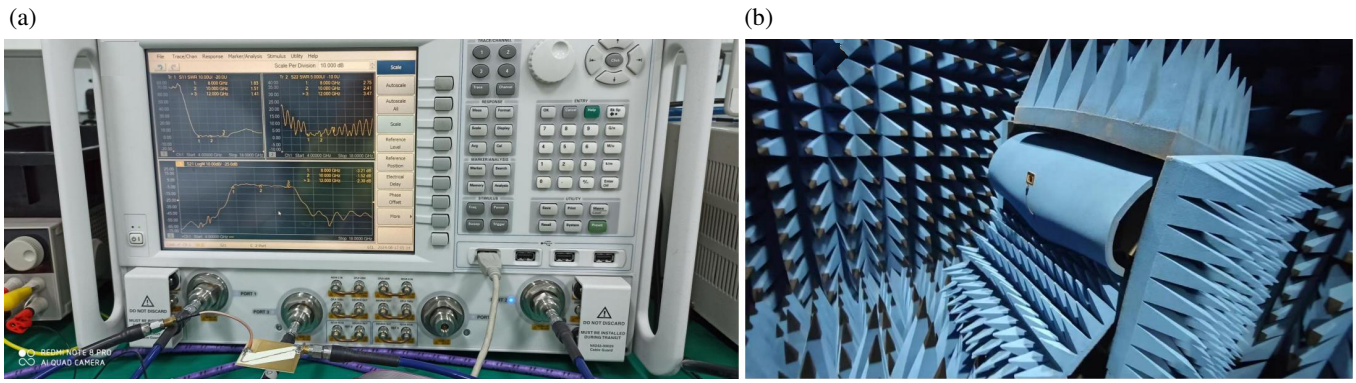

FIGURE 8. Measurement setup. (a) For S-parameters of the antenna, the BPF, and the integrated filter antenna. (b) For radiation patterns of the filter antenna.

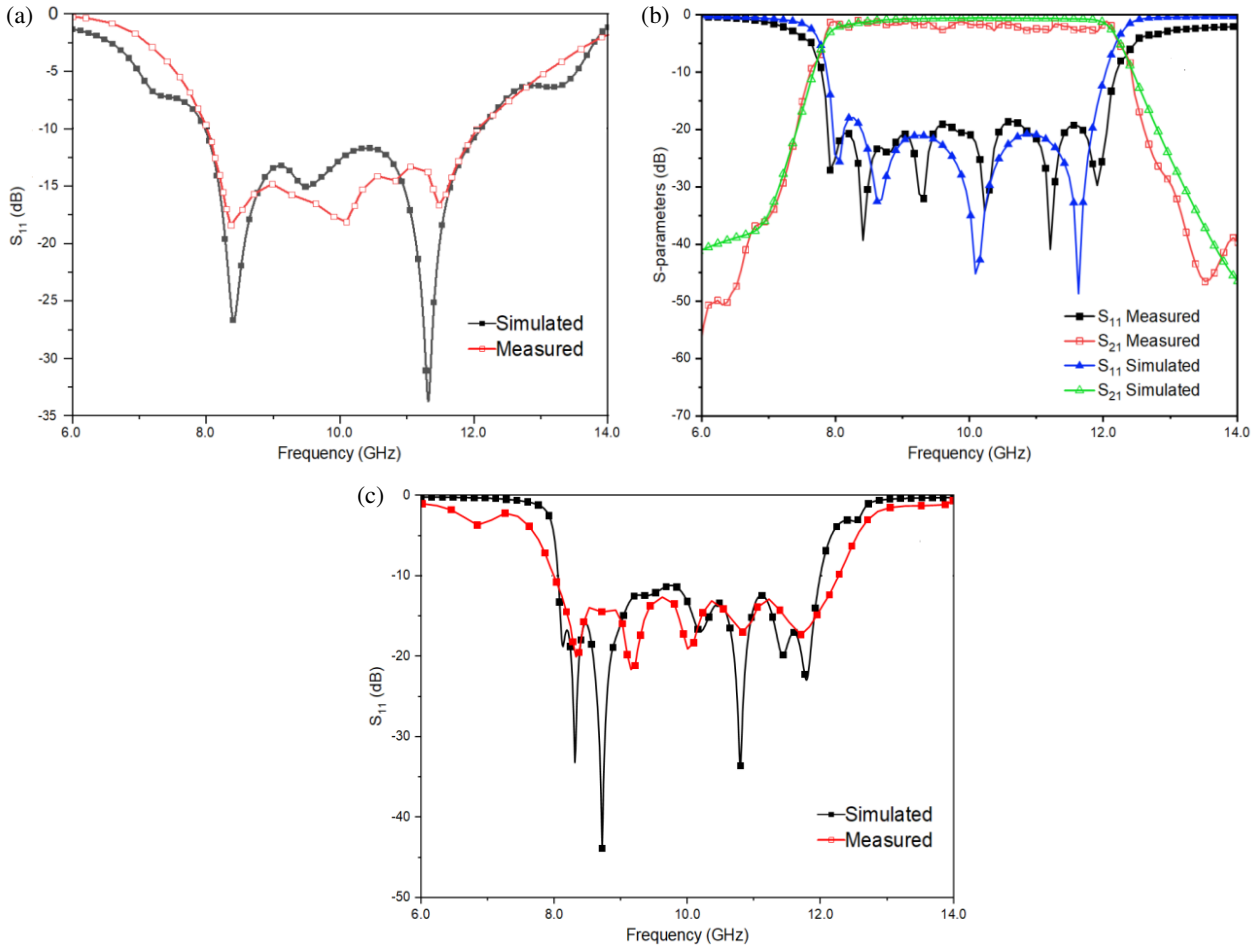

FIGURE 9. Comparison of the measured and simulated S-parameters. (a) S_{11} for the antenna. (b) S-parameters for the BPF. (c) S_{11} for the integrated filter antenna.

width of the integrated system has expanded, with the measured results ranging from 7.99 to 12.02 GHz compared to the simulated range of 8.06 to 11.99 GHz.

Figures 10(a) to (d) illustrate the radiation patterns of the integrated filter antenna. A notable observation is that the measured radiation patterns show slightly higher peak gains (for example, 6.85 dBi at 11.5 GHz) than the simulated ones. The slightly higher measured peak gain is likely attributable to fabrication tolerances, assembly errors, connector and cable effects, and uncertainties in the measurement environment, rather than indicating a definite enhancement in radiation efficiency. Nevertheless, the measured and simulated radiation patterns remain in good agreement, confirming the stable radiation behavior of the integrated filter antenna across the operating band.

The measured results confirm that the integrated filter antenna provides a clear performance improvement by incorpo-

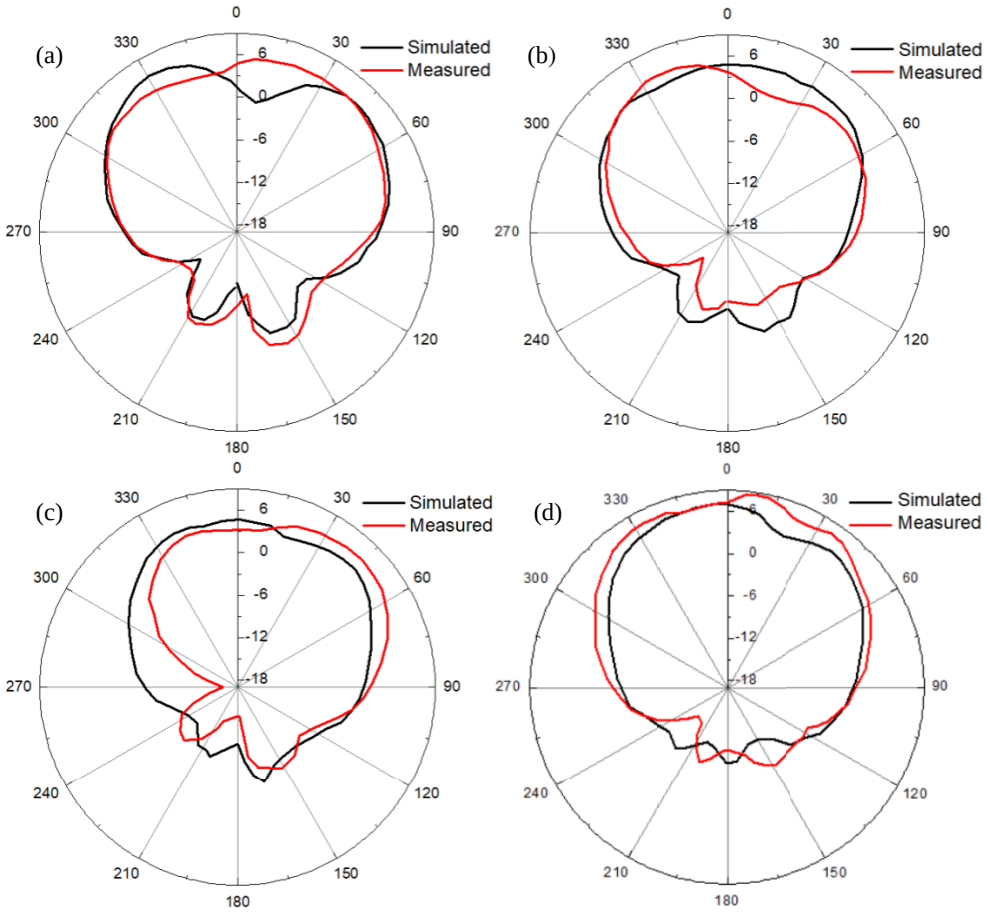

FIGURE 10. Comparison of the measured and simulated radiation patterns. (a) 8.5 GHz, (b) 9 GHz, (c) 10 GHz, and (d) 11.5 GHz.

TABLE 1. Comparison with other designs.

Ref.	Freq. (GHz)	BW (%)	Peak gain (dBi)	Size (λ_0)
[24]	2.19–2.68	20.1	9.5	$1.2 \times 1.2 \times 0.032$
[28]	8.30–12.29, 12.91–14.21	38.75 (X), 9.58 (Ku)	7.13	0.53 (X-band)
[31]	9.71–11.41	15.92	5.71	/
[32]	2–3.5	54.5	2.3	$0.41 \times 0.45 \times 0.01$
[33]	4.45–5.52	21.5	4.8	0.4×0.4
[34] (1 element)	6.26–7.4	17	9.7	$1.11 \times 0.68 \times 0.0457$
[35]	2.74–3.86	33.94	9.2	$1.21 \times 1.21 \times 0.94$
The proposed design	7.99–12.02	40.3	6.85	$1.17 \times 1.17 \times 0.12$

rating the desired filtering functionality. Unlike the dual-band antenna in [28], which focused solely on radiation, this work achieves robust out-of-band rejection greater than 20 dB, effectively suppressing harmonics and interferers. This key feature, combined with a 45.27% reduction in patch area and a measured peak gain of 6.85 dBi, underscores the system-level improvement attained through co-design.

Table 1 compares the proposed integrated filter antenna with other state-of-the-art designs reported in the literature. The proposed antenna operates over 7.99–12.02 GHz and achieves a wide fractional bandwidth of 40.3%, which is significantly broader than those of most referenced designs, such as [31] (15.92%) and [33] (21.5%). In addition, the proposed design exhibits a competitive peak gain of 6.85 dBi, outperforming [32] (2.3 dBi) and [33] (4.8 dBi), while remaining comparable to higher-gain designs such as [24] (9.5 dBi) and [34] (9.7 dBi). In terms of size, the proposed antenna is compact, more space-efficient than [34], and comparable to [24]. Overall, the proposed design achieves a favorable balance among wide bandwidth, competitive gain, and compact size, demonstrating strong potential for modern wireless communication systems requiring high efficiency and miniaturization.

As illustrated in Fig. 6, the final antenna patch (including the feeder) exhibits a 45.27% reduction in size compared to the original side-fed monopole antenna. The dimensions provided in Table 1 represent the overall integrated filter antenna. If only the effective surface area of the antenna is considered, the proposed design demonstrates even greater dimensional advantages.

5. CONCLUSIONS

This work represents a systematic development of 3D integrated radiating structures, extending a high-performance antenna into a complete filtering antenna system through the monolithic integration of a slotted patch antenna and a seventh-order microstrip bandpass filter within a compact multilayer structure employing vertical interconnects. The design incorporates several key features, including an air cavity surrounded by VIAs, which functions as an effective shielding wall to reduce dielectric loss, suppress backward radiation, and enhance front-to-back isolation. Furthermore, structural modifications to the radiating patch, including optimized asymmetric feeding, slotting, and chamfering, were implemented to lower the resonant frequency and extend the bandwidth, achieving a notable size reduction of 45.27% compared to an initial side-fed monopole.

Measurement results demonstrate that the integrated prototype achieves a wide operating bandwidth of 40.3% (7.99–12.02 GHz) with a peak gain of 6.85 dBi, showing good agreement with simulations. The design successfully combines the advantages of compact size ($1.17\lambda_0 \times 1.17\lambda_0 \times 0.12\lambda_0$), wideband operation, and effective harmonic suppression, confirming the proposed architecture as a highly promising solution for modern X-band wireless systems demanding high integration, minimal footprint, and directional radiation characteristics. Future work will further exploit this 3D integration platform to investigate additional miniaturization, multiband operation, and the integration of active RF components toward a more complete system-on-package (SoP) front-end.

ACKNOWLEDGMENTS

This work was supported by the Southwest Minzu University Research Startup Funds (No. RQD2024009, RQD2021060) and the Sichuan Provincial Science and Technology Department Key Project (No. 2025YFHZ0013).

REFERENCES

[1] Sun, F., X. Wu, N. Ou, Y. Luan, and W. Yu, "A dual-band X/Ku copolarized shared-aperture waveguide slot antenna," *IEEE Antennas and Wireless Propagation Letters*, Vol. 23, No. 12, 4418–4422, 2024.

[2] Lim, E. H. and K. W. Leung, *Compact Multifunctional Antennas for Wireless Systems*, John Wiley & Sons, 2012.

[3] Tang, J. and H. Liu, "An efficient dual-band filter-antenna design based on simplified integration methodology," *International Journal of RF and Microwave Computer-Aided Engineering*, Vol. 29, No. 6, e21704, 2019.

[4] Rodrigues, L., T. Varum, and J. N. Matos, "The application of reconfigurable filtennas in mobile satellite terminals," *IEEE Access*, Vol. 8, 77 179–77 187, 2020.

[5] Dorairajan, N. and C. M. Perumal, "Implementation and parametric analysis of single and dual band planar filtering antennas for WLAN applications," *Wireless Networks*, Vol. 26, No. 8, 5883–5895, 2020.

[6] Xue, K., D. Yang, C. Guo, H. Zhai, H. Li, and Y. Zeng, "A dual-polarized filtering base-station antenna with compact size for 5G applications," *IEEE Antennas and Wireless Propagation Letters*, Vol. 19, No. 8, 1316–1320, 2020.

[7] Yang, K., M.-H. Hoang, X. Bao, P. McEvoy, and M. J. Ammann, "Dual-stub Ka-band Vivaldi antenna with integrated bandpass filter," *IET Microwaves, Antennas & Propagation*, Vol. 12, No. 5, 668–671, 2018.

[8] Mao, C.-X., S. Gao, Y. Wang, F. Qin, and Q.-X. Chu, "Multimode resonator-fed dual-polarized antenna array with enhanced bandwidth and selectivity," *IEEE Transactions on Antennas and Propagation*, Vol. 63, No. 12, 5492–5499, 2015.

[9] Jiang, Z. H. and D. H. Werner, "A compact, wideband circularly polarized co-designed filtering antenna and its application for wearable devices with low SAR," *IEEE Transactions on Antennas and Propagation*, Vol. 63, No. 9, 3808–3818, 2015.

[10] Zuo, J., X. Chen, G. Han, L. Li, and W. Zhang, "An integrated approach to RF antenna-filter co-design," *IEEE Antennas and Wireless Propagation Letters*, Vol. 8, 141–144, 2009.

[11] Lovato, R. and X. Gong, "A third-order SIW-integrated filter/antenna using two resonant cavities," *IEEE Antennas and Wireless Propagation Letters*, Vol. 17, No. 3, 505–508, 2018.

[12] Feng, W., Y. Feng, W. Yang, W. Che, and Q. Xue, "High-performance filtering antenna using spoof surface plasmon polaritons," *IEEE Transactions on Plasma Science*, Vol. 47, No. 6, 2832–2837, 2019.

[13] Chuang, C.-T. and S.-J. Chung, "Synthesis and design of a new printed filtering antenna," *IEEE Transactions on Antennas and Propagation*, Vol. 59, No. 3, 1036–1042, 2011.

[14] Wu, W.-J., Y.-Z. Yin, S.-L. Zuo, Z.-Y. Zhang, and J.-J. Xie, "A new compact filter-antenna for modern wireless communication systems," *IEEE Antennas and Wireless Propagation Letters*, Vol. 10, 1131–1134, 2011.

[15] Chen, X., F. Zhao, L. Yan, and W. Zhang, "A compact filtering antenna with flat gain response within the passband," *IEEE Antennas and Wireless Propagation Letters*, Vol. 12, 857–860, 2013.

[16] Hsieh, C.-Y., C.-H. Wu, and T.-G. Ma, "A compact dual-band filtering patch antenna using step impedance resonators," *IEEE Antennas and Wireless Propagation Letters*, Vol. 14, 1056–1059, 2015.

[17] Nova, O. A., J. C. Bohorquez, N. M. Pena, G. E. Bridges, L. Shafai, and C. Shafai, "Filter-antenna module using substrate integrated waveguide cavities," *IEEE Antennas and Wireless Propagation Letters*, Vol. 10, 59–62, 2011.

[18] Yusuf, Y., H. Cheng, and X. Gong, "A seamless integration of 3-D vertical filters with highly efficient slot antennas," *IEEE Transactions on Antennas and Propagation*, Vol. 59, No. 11, 4016–4022, 2011.

[19] Jin, J. Y., S. Liao, and Q. Xue, "Design of filtering-radiating patch antennas with tunable radiation nulls for high selectivity," *IEEE Transactions on Antennas and Propagation*, Vol. 66, No. 4, 2125–2130, 2018.

[20] Yang, W., M. Xun, W. Che, W. Feng, Y. Zhang, and Q. Xue, "Novel compact high-gain differential-fed dual-polarized filtering patch antenna," *IEEE Transactions on Antennas and Propa-*

gation, Vol. 67, No. 12, 7261–7271, 2019.

[21] Pan, Y. M., P. F. Hu, X. Y. Zhang, and S. Y. Zheng, "A low-profile high-gain and wideband filtering antenna with metasurface," *IEEE Transactions on Antennas and Propagation*, Vol. 64, No. 5, 2010–2016, 2016.

[22] Liu, Q., L. Zhu, J. Wang, and W. Wu, "A wideband patch and SIW cavity hybrid antenna with filtering response," *IEEE Antennas and Wireless Propagation Letters*, Vol. 19, No. 5, 836–840, 2020.

[23] Xu, K., J. Shi, X. Qing, and Z. N. Chen, "A substrate integrated cavity backed filtering slot antenna stacked with a patch for frequency selectivity enhancement," *IEEE Antennas and Wireless Propagation Letters*, Vol. 17, No. 10, 1910–1914, 2018.

[24] Yang, D., H. Zhai, C. Guo, and H. Li, "A compact single-layer wideband microstrip antenna with filtering performance," *IEEE Antennas and Wireless Propagation Letters*, Vol. 19, No. 5, 801–805, 2020.

[25] Ding, C. F., X. Y. Zhang, Y. Zhang, Y. M. Pan, and Q. Xue, "Compact broadband dual-polarized filtering dipole antenna with high selectivity for base-station applications," *IEEE Transactions on Antennas and Propagation*, Vol. 66, No. 11, 5747–5756, 2018.

[26] Zhang, X. Y., W. Duan, and Y.-M. Pan, "High-gain filtering patch antenna without extra circuit," *IEEE Transactions on Antennas and Propagation*, Vol. 63, No. 12, 5883–5888, 2015.

[27] Yang, W., S. Chen, Q. Xue, W. Che, G. Shen, and W. Feng, "Novel filtering method based on metasurface antenna and its application for wideband high-gain filtering antenna with low profile," *IEEE Transactions on Antennas and Propagation*, Vol. 67, No. 3, 1535–1544, 2019.

[28] Yan, N., K. Ma, H. Zhang, and P. Jia, "An SISL triple-band multimode stacked-patch antenna with L-strips for multiband applications," *IEEE Transactions on Antennas and Propagation*, Vol. 67, No. 2, 1284–1288, 2019.

[29] Ma, K., N. Yan, and Y. Wang, "Recent progress in SISL circuits and systems: Review of passive and active circuits demonstrating SISL's low loss and self-packaging and showcasing the merits of metallic, shielded, suspended lines," *IEEE Microwave Magazine*, Vol. 22, No. 4, 49–71, 2021.

[30] Wang, J., T. Tang, T. S. Almoneef, and M. A. Aldhaeebi, "X/Ku-band antenna with integrated back cavity for directional radiation," *Progress In Electromagnetics Research C*, Vol. 158, 171–177, 2025.

[31] Zhang, X., T. Tang, M. A. Aldhaeebi, and T. S. Almoneef, "Novel design and implementation of 3D packaged wideband bandpass filters," *Scientific Reports*, Vol. 14, No. 1, 23584, 2024.

[32] Althuwayb, A. A., D. Chaturvedi, and A. Kumar, "Substrate integrated waveguide (SIW) cavity-backed slot antenna with monopole-like radiation for vehicular communications," *Applied Physics A*, Vol. 128, No. 3, 202, 2022.

[33] Chen, B.-J., X.-S. Yang, and B.-Z. Wang, "A compact high-selectivity wideband filtering antenna with multipath coupling structure," *IEEE Antennas and Wireless Propagation Letters*, Vol. 21, No. 8, 1654–1658, 2022.

[34] Zhang, J., L. Li, Y. He, and L. Zhang, "A novel wideband filtering antenna for sub-6 GHz 5G base station application," in *2022 IEEE MTT-S International Microwave Workshop Series on Advanced Materials and Processes for RF and THz Applications (IMWS-AMP)*, 1–3, Guangzhou, China, 2022.

[35] Yin, W., J. Si, Z. Deng, C. Li, and S. K. Khamas, "A compact coupling-fed omnidirectional wideband filtering antenna with high selectivity," *Electromagnetics*, Vol. 44, No. 7, 521–532, 2024.